

A nano-confined source based on surface plasmon Bragg reflectors and nanocavity

Qingyan Wang*, Jia Wang, Shulian Zhang

Key Laboratory of Precision Measurement Technology and Instruments,
Department of Precision Instruments, Tsinghua University, Beijing, 100084, China
*wangqy03@mails.tsinghua.edu.cn

Abstract: A type of nano-confined light source based on SPP Bragg reflectors and a nanocavity has been realized. The structures consisting of a nanocavity surrounded by annular grooves are used to obtain a single, localized and non-radiating central peak, which can be used as a nano source. Characterization of the SPP field in the vicinity of the samples with different structural parameters is accomplished by the scanning near-field optical microscope (SNOM), demonstrating the ability of the structures to enhance the peak intensity and to suppress the sidelobes. During 600nm distance away from the sample surface, the FWHM of the central peak is below 285nm (0.45λ), and the modifications of the structural parameters result in at least 1.27 times enhancement of the central peak intensity together with the sidelobe suppression of no more than 73% of the central peak intensity. Numerical simulations based on FDTD method show a good agreement with the experimental results, and give some clues to understand the physical mechanisms behind these phenomena. This type of SPP-based nano source is promising to be applied in near-field imaging, data storage, optical manipulation and localized spectrum detection.

©2008 Optical Society of America

OCIS codes: (240.0240) Optics at surfaces; (240.6680) Surface plasmons; (180.4243) Near-field microscopy.

References and links

1. D. W. Pohl, W. Denk, and M. Lanz, "Optical stethoscopy: Image recording with resolution $\lambda/20$," *Appl. Phys. Lett.* **44**, 651-653 (1984).
2. E. Betzig, J. K. Trautman, T. D. Harris, J. S. Weiner, and R. L. Kostelak, "Breaking the diffraction barrier: optical microscopy on a nanometric scale," *Science* **251**, 1468-1470 (1991).
3. A. Partovi, D. Peale, M. Wuttig, C. A. Murray, G. Zydzik, L. Hopkins, K. Baldwin, W. S. Hobson, J. Wynn, J. Lopata, L. Dhar, R. Chichester, and J. H. J. Yeh, "High-power laser light source for near-field optics and its application to high-density optical data storage," *Appl. Phys. Lett.* **75**, 1515-1517 (1999).
4. K. Tanaka and M. Tanaka, "Simulation of confined and enhanced optical near-fields for an I-shaped aperture in a pyramidal structure on a thick metallic screen," *J. Appl. Phys.* **95**, 3765-3771 (2004).
5. E. X. Jin and X. Xu, "Enhanced optical near field from a bowtie aperture," *Appl. Phys. Lett.* **88**, 153110-1-3 (2006).
6. F. Zenhausern, M. P. O. Boyle, and H. K. Wickramasinghe, "Apertureless near-field optical microscope," *Appl. Phys. Lett.* **65**, 1623-1625 (1994).
7. Y. Inouye and S. Kawata, "Near-Field Scanning Optical Microscope With A Metallic Probe Tip," *Opt. Lett.* **19**, 159-161 (1994).
8. L. Novotny, D. W. Pohl, and B. Hecht, "Scanning Near-Field Optical Probe With Ultrasmall Spot Size," *Opt. Lett.* **20**, 970-972 (1995).
9. T. Grosjean and D. Courjon, "Immaterial tip concept by light confinement," *J. Microsc.* **202**, 273-278 (2001).
10. T. Grosjean, D. Courjon, and D. Van Labeke, "Bessel beams as virtual tips for near-field optics," *J. Microsc.* **210**, 319-323 (2003).
11. T. Hong, J. Wang, L. Sun, and D. Li, "Numerical simulation analysis of a near-field optical virtual probe," *Appl. Phys. Lett.* **81**, 3452-3454 (2002).
12. T. Hong, J. Wang, L. Sun, and D. Li, "Numerical and experimental research on the near-field optical virtual probe," *Scanning* **26**, 57-62 (2004).

13. M. I. Stockman, "Nanofocusing of Optical Energy in Tapered Plasmonic Waveguides," *Phys. Rev. Lett.* **93**, 137404-1-4 (2004).
14. N. A. Janunts, K. S. Baghdasaryan, K. V. Nerkararyan, and B. Hecht, "Excitation and superfocusing of surface plasmon polaritons on a silver-coated optical fiber tip," *Opt. Commun.* **253**, 118-124 (2005).
15. B. Wang and G. P. Wang, "Plasmon Bragg reflectors and nanocavities on flat metallic surfaces," *Appl. Phys. Lett.* **87**, 013107-1-3 (2005).
16. T. A. Kelf, Y. Sugawara, R. M. Cole, J. J. Baumberg, M. E. Abdelsalam, S. Cintra, S. Mahajan, A. E. Russell, and P. N. Bartlett, "Localized and delocalized plasmons in metallic nanovoids," *Phys. Rev. B* **74**, 245415-1-12 (2006).
17. K. G. Dmitri, F. P. P. David, W. V. Michael, and Z. Xiang, "Local electric field enhancement during nanofocusing of plasmons by a tapered gap," *Phys. Rev. B* **75**, 035431-1-5 (2007).
18. D. Peyrade, E. Silberstein, P. Lalanne, A. Talneau, and Y. Chen, "Short Bragg mirrors with adiabatic modal conversion," *Appl. Phys. Lett.* **81**, 829-831 (2002).
19. J. R. Krenn, H. Ditlbacher, G. Schider, A. Hohenau, A. Leitner, and F. R. Aussenegg, "Surface plasmon micro- and nano-optics," *J. Microsc.* **209**, 167-172 (2003).
20. J.-C. Weeber, Y. Lacroute, A. Dereux, E. Devaux, T. Ebbesen, C. Girard, and M. U. González and A.-L. Baudrion, "Near-field characterization of Bragg mirrors engraved in surface plasmon waveguides," *Phys. Rev. B* **70**, 235406-1-12 (2004).
21. M. U. Gonzalez, J. C. Weeber, A. L. Baudrion, A. Dereux, A. L. Stepanov, J. R. Krenn, E. Devaux, and T. W. Ebbesen, "Design, near-field characterization, and modeling of 45° surface-plasmon Bragg mirrors," *Phys. Rev. B* **73**, 155416-1-13 (2006).
22. E. Descrovi, V. Paeder, L. Vaccaro, and H.-P. Herzig, "A virtual optical probe based on localized surface plasmon polaritons," *Opt. Express* **13**, 7017-7027 (2005).
<http://www.opticsexpress.org/abstract.cfm?URI=OPEX-13-18-7017>.
23. B. Hu, J. Liu, B.-y. Gu, S. Di, X.-d. Sun, and S.-q. Wang, "Enhanced effect of local fields in subwavelength metallic series nanocavities from surface plasmon polaritons," *J. Opt. Soc. Am. A. Opt. Image. Sci. Vis.* **24**, A1-6 (2007).
24. G. Yiyang and V. Jelena, "Design of plasmon cavities for solid-state cavity quantum electrodynamics applications," *Appl. Phys. Lett.* **90**, 033113-1-3 (2007).
25. C. L. Nathan, L. Antoine, and O. Sang-Hyun, "Periodic modulation of extraordinary optical transmission through subwavelength hole arrays using surrounding Bragg mirrors," *Phys. Rev. B* **76**, 155109-1-5 (2007).
26. C. L. Nathan, L. Antoine, and O. Sang-Hyun, "Lateral confinement of surface plasmons and polarization-dependent optical transmission using nanohole arrays with a surrounding rectangular Bragg resonator," *Appl. Phys. Lett.* **91**, 253105-1-3 (2007).
27. J. C. Weeber, A. Bouhelier, G. ColasdesFrans, L. Markey, and A. Dereux, "Submicrometer In-Plane Integrated Surface Plasmon Cavities," *Nano. Lett.* **7**, 1352-1359 (2007).
28. J. C. Weeber, A. Bouhelier, G. C. d. Frans, S. Massenot, J. Grandidier, L. Markey, and A. Dereux, "Surface-plasmon hopping along coupled coplanar cavities," *Phys. Rev. B* **76**, 113405-1-4 (2007).
29. K. Askin, S. S. Senlik, and A. Atilla, "Plasmonic band gap cavities on biharmonic gratings," *Phys. Rev. B* **77**, 195130-1-7 (2008).
30. C. Ding, X. Hu, P. Jiang, and Q. Gong, "Tunable surface plasmon polariton microcavity," *Phys. Rev. A* **372**, 4536-4538 (2008).
31. Q. Wang, J. Wang, and S. Zhang, "Confined optical fields based on surface plasmon polaritons," *Proc. SPIE* **6831**, 68310T-1-6 (2007).
32. Q. Wang, J. Wang, and S. Zhang, "Confined optical field based on surface plasmon polaritons and the interactions with nano-spheres," *J. Opt. Soc. Am. B* **25**, 1096-1104 (2008).
33. L. Novotny and B. Hecht, *Principles of Nano-optics* (Cambridge U. Press, Cambridge, 2006).
34. W. L. Barnes, T. W. Preist, S. C. Kitson, and J. R. Sambles, "Physical origin of photonic energy gaps in the propagation of surface plasmons on gratings," *Phys. Rev. B* **54**, 6227-6244 (1996).

1. Introduction

A nano light source is an essential device in near-field imaging, data-storage, optical manipulation and localized spectrum detection. Two main types of nano sources are currently used in near-field optics. One type of source is aperture source, including aperture probe [1, 2] and very small aperture laser (VSAL) [3-5]. Although a high resolution can be achieved by such aperture sources, the output field is radiating and diverges very quickly, which requires the distance between sources and samples be rigorously controlled below 50nm. The other type of nano source is the sharp tip [6-8], referred to as apertureless source. The optical intensity is locally enhanced at the tip and forms a nano source with higher resolution than the aperture source. However, the localized field attenuates rapidly and the working distance is no more than 10nm, even smaller than that of the aperture source.

In order to relax the working distance requirement, a non-radiating confined optical field based on the interference of evanescent waves is proposed [9, 10]. The zero-order mode in the evanescent interference pattern can keep less than half of wavelength during the distance range about wavelength [11, 12]. Such confined optical field can be used as a nano source, and the separation regulation can be relaxed. Nevertheless, the intensity of the zero-order mode in the interference field is not high enough (no more than 10% of the maximal intensity of the incident light), and the high-order modes (namely sidelobes) in the interference field are undesired. Low peak intensity and high sidelobes are obstacles in practical applications. One solution to these problems is to introduce surface plasmon polaritons (SPPs) excited on corrugated metallic surface. With proper SPP-based nanophotonics elements, efficient transformations of traveling delocalized SPPs into highly localized excitations can be realized to achieve a confined source [13-17]. Among these SPP-based elements, the metal gratings with plasmonic band gap (PBG) are attractive. The gratings with a period meeting the Bragg reflection condition can constructively reflect SPP waves and behave as an efficient Bragg mirror [18-21]. A singular defect in such periodic structure will show cavity-like effect [15, 22-30]. Thus, SPP resonance can be reflected by the Bragg reflectors around the cavity and then localized in the cavity. E. Descrovi and L. Vaccaro et al. reported the confinement effect of a SPP microcavity constructed by two metallic distributed Bragg reflectors with a sinusoidal profile, and indicated that the zero-order cavity mode is enhanced to be used as a nano source [22]. Recently, Y. Gong and J. Vuckovic investigated the influence of the length of a SPP microcavity with a rectangular profile on the electric field distribution [24]. Subsequently, N. C. Lindquist et al. studied theoretically and experimentally the polarization-dependent confinement effect of a SPP microcavity surrounded by square-shaped Bragg mirrors [25, 26]. Meanwhile, J. C. Weeber et al. measured the near-field distributions of SPP microcavities [27] and obtained SPP “hopping” along coupled coplanar cavities [28]. These works mainly concerned the confinement of the electric field and the influences of the SPP cavity length. However, the influences of other structural parameters on the electric field distributions are rarely reported, and the realization of a single peak with small sidelobes, which can be used as an optimized nano source, has still been lacking.

For achieving a single enhanced peak and suppressed sidelobes with SPP nanocavity structure, we have numerically investigated the factors that influence the SPP field distributions, and demonstrated that the sidelobes intensity can be decreased by adjusting the structural parameters of the nanocavity, which allows us to optimize the structure to produce a high-intensity nano source with smaller sidelobes [31, 32]. In this paper, we present the results of experimental investigations to verify this idea. The SPP confined field is generated in a nanocavity surrounded by annular grooves with the period satisfying the following expression:

$$k_{\text{SPP}}a = \pi. \quad (1)$$

where a is the period of the annular grooves, and k_{SPP} holds for the in-plane plasmon wavevector. We compare two structures with different structural parameters of the cavities, and with these structures we exploit the optimization of the distribution of the nano source by adjusting the cavity parameters.

2. Experimental results

The annular grooves are prepared with a FEI Dual Beam Focused Ion Beam in 50nm-thick gold films evaporated on BK7 substrates. The fabricated structures consist of 30 annular grooves with the period a satisfying equation (1). The central area is treated as a nanocavity with the length of $L=1.5a$. The depth and the width of the innermost groove are defined as d and w , respectively, and vary for different structures (see Fig.1). The setup for SPP excitation and near-field measurement is described in Fig. 2. The samples are excited with linear polarized focused hollow beam of 2.06mW, which is produced by injecting a 38mW He-Ne laser ($\lambda=632.8\text{nm}$) into an annular diaphragm and then focusing by an objective with

$NA=1.25$. The incident angle can be adjusted by moving the annular diaphragm along the optical axis to ensure the SPP resonance angle to be obtained. The SPP field localized in the nanocavity is mapped by a scanning near-field optical microscope (SNOM). A tapered optical fiber coated with a thin layer of aluminum is attached to a tuning fork, and the separation regulation is controlled by the shear-force technology. The optical signal picked up by the fiber tip is then converted by a photomultiplier tube and amplified in a lock-in amplifier. When the tip is scanned in the near-field zone, the signal collected by the probe provides the spatial distribution of the optical near-field intensity in a plane parallel to the sample surface.

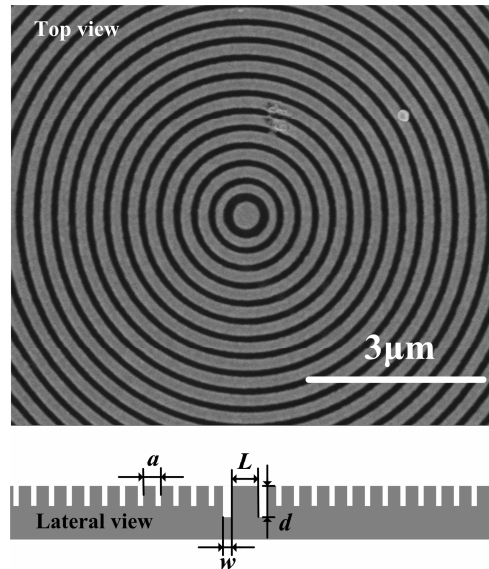


Fig.1. SEM image and schematic diagram of the structures characterized by the period of the rings of $a=310\text{nm}$. The depth and the width of the rings (except the innermost one) are 20nm and 100nm, respectively. The parameters used in the definition of the cavity and the innermost ring are also shown.

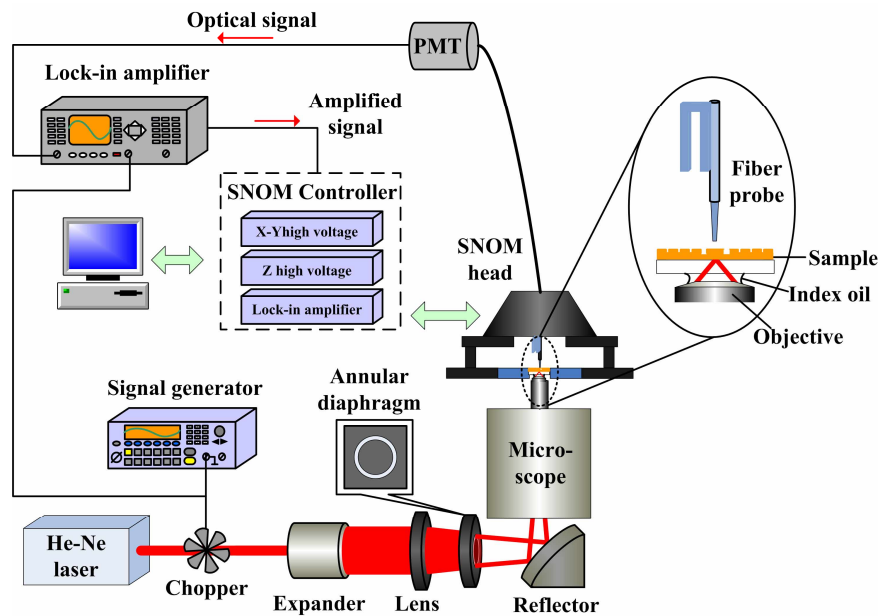


Fig. 2. Experimental setup used to excite SPPs and measure the near-field distributions.

In the first case we study a smooth gold film without any structures on the surface. The calculated $|E|^2$ and $|E_z|^2$ of the SPP field on the film surface excited by linear polarized focused hollow beam are shown in Fig. 3(a) and (b), respectively. Both the images are normalized. It can be seen that the longitudinal component contributes to the excitation of SPPs and dominates the total field. The field distribution measured by the probe tip with the tip-surface distance of $\sim 5\text{nm}$ is mapped in Fig. 3(c). The maximal intensity is 6.13. To compare with the calculated intensity distributions, the experimental image is also normalized. Because of the symmetry of the HE_{11} mode propagating in the core of an aperture near-field probe [33], our experiment is predominantly sensitive to $|E_z|^2$, the field distributions of which show a good agreement near the center of the focused area, as indicated in Fig. 3(b), (c) and (d). The average FWHM (full width at half maximal) of the two main peaks at the center of the focused area is 230nm in Fig. 3(b) and 228nm in Fig. 3(c), respectively. However, there is a discrepancy in the distributions of sidelobes intensity. The bright spots around the two main peaks in Fig. 3(c) are mainly due to the scattering of the film surface imperfections and flaws. The inhomogeneous thickness of the film also influences the SPP field. Moreover, the vibration in the scanning and the field disturbance by the probe tip inevitably make some differences between experimental and theoretical results.

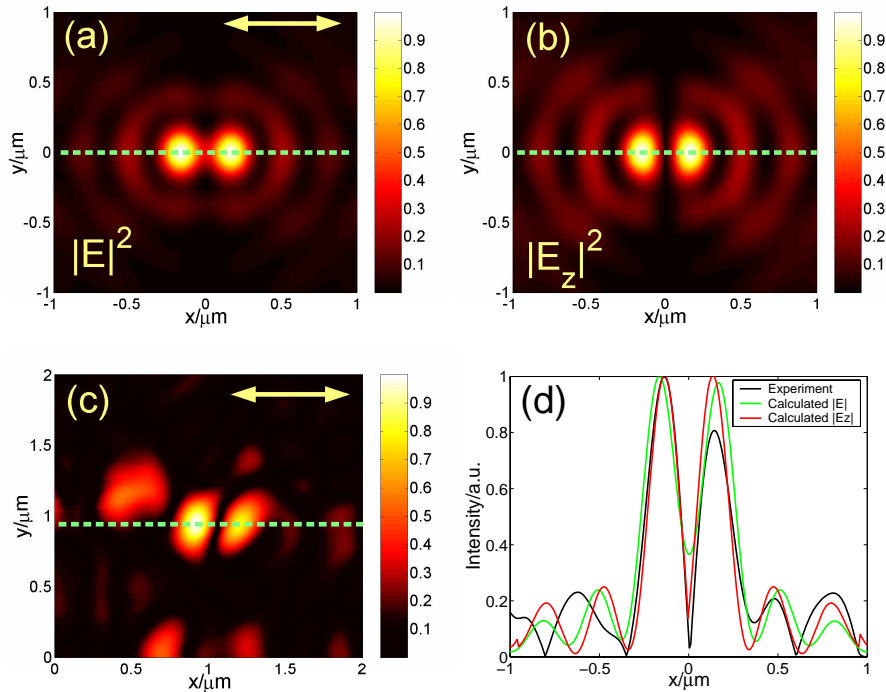


Fig. 3. Intensity distributions of the SPP field on the smooth gold film excited by linear polarized focused hollow beam. The polarization direction of the illumination is indicated by the double arrow. (a) Calculated distribution of $|E|^2$ on the film surface (Normalized). (b) Calculated distribution of $|E_z|^2$ on the film surface (Normalized). (c) Near-field image with the tip-surface distance of $\sim 5\text{nm}$ (Normalized). (d) Cross-sections of the SPP field, as indicated by the dashed lines in (a), (b) and (c) - obtained by NT-MDT SNOM system

Note that both calculation and experiment show two lobes in the center, which makes the field unusable to generate a single, localized and non-radiating nano source. In order to obtain one single peak, a nanocavity surrounded by annular grooves is designed. The period of the annular grooves is $a = \lambda_{\text{SPP}}/2 = 310\text{nm}$, and the length of the cavity is $L = 1.5a = 465\text{nm}$. The structural parameters of the innermost groove are $d = 20\text{nm}$ and $w = 100\text{nm}$, the same as other grooves. We refer to this structure as *Structure 1*. The field distribution measured by the probe

tip with the tip-surface distance of $\sim 5\text{nm}$ is mapped in Fig. 4(a). It is seen that this type of structure is rather efficient in reflecting and localizing SPP beams and thereby confining the excited SPP field into one peak at the cavity area. For quantitatively characterizing the SPP localization ability of the nanocavity, we consider three near-field parameters: FWHM of the central peak, maximal intensity of the central peak (defined as P), and a coefficient r to describe the extent of sidelobe suppression effect, which is expressed as

$$r = (E_s / E_c) \times 100\%. \quad (2)$$

where E_s is the maximal intensity of sidelobes and E_c is the maximal intensity of the central peak. Fig. 4(b) shows the cross-section along the dashed line in Fig. 4(a). It can be seen that the FWHM of the central peak is 275nm (0.44λ) and the maximal intensity of the central peak P is 11.27 , which is about 1.8 times of the maximal intensity on the smooth gold film. The sidelobe suppression parameter r is determined according to the intensity map in Fig. 4(a) (note that r cannot be determined according to the cross-section in Fig. 4(b), because the maximal sidelobe intensity is not on the dashed line in Fig. 4(a)). The value of r is 45.8% .

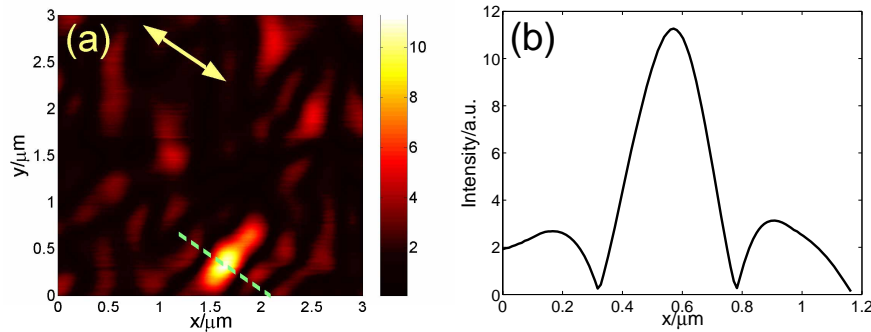


Fig. 4. Intensity distribution of the SPP field on the surface of *Structure 1* with $a=310\text{nm}$, $L=465\text{nm}$, $d=20\text{nm}$ and $w=100\text{nm}$. (a) Near-field image with the tip-sample distance of $\sim 5\text{nm}$. The polarization direction of the illumination is indicated by the double arrow. (b) Cross-section of (a), as indicated by the dashed line.

The SPP localization by the nanocavity is based on the SPP Bragg reflection. The cavity can be considered as a resonator, and the periodical grooves just play a role of Bragg grating, serving as a mirror-reflector for the SPPs propagating in-plane. The coupling between the optical field and SPPs becomes strong when the resonant length of the resonator and the period of the Bragg grating satisfy the expression

$$L = \frac{(2n+1)}{2} a, n = 1, 2, 3, \dots \quad (3)$$

Due to the attenuation of SPPs during the propagation in-plane, the strongest enhancement appears in the lowest-order cavity mode, corresponding to $L=1.5a$, while other cavity modes are blocked. The lowest-order mode forms an interference pattern at the nanocavity area and shows a clear central peak in the near-field distribution, which can be used as a near-field nano source, as shown in Fig. 4(a).

3. Optimization of the nano source

The presence of sidelobes surrounding the central peak is undesirable for nano source applications. It has been investigated that the intensity of sidelobes is directly related to the depth of the grooves [22, 30]. As the groove depth increases, the sidelobes are reduced. Unfortunately, a large depth introduces strong perturbations of the SPP mode, leading to an increase in scattered light. In order to achieve a trade-off, we only modify the depth of the innermost groove, denoted by d as above mentioned. The numerical simulations by FDTD

method (detailed discussion is described in Ref [32]) show that with d more than 30nm, increasing d results in a decrease of the sidelobe intensity together with dramatic damping of the central peak intensity (Fig. 5(a)). Keeping d at 30nm, the next step is to do further design to obtain an optimized nano source. The intensities of central peak and sidelobes are also related to the width of the groove [30, 34]. Following this idea, we investigate the influences of width of the innermost groove (defined as w) on the near-field parameters of the nano source, and prove that with the proper selection of w , strongest central peak and lowest sidelobes can be achieved simultaneously. The results are shown in Fig. 5(b), and the optimized value is $w=0.5a$.

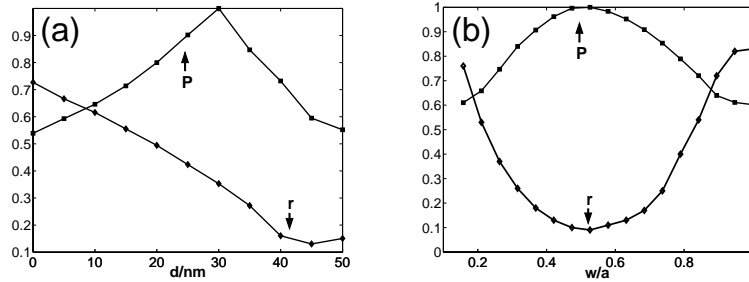


Fig. 5. Numerical investigations of the influences of the depth and the width of the innermost groove (described as d and w , respectively). $L=1.5a$ and the distance between the sample surface and the calculation plane is 200nm. (a) Maximal intensity of the central peak P and sidelobe suppression r versus d with $w=100$ nm. (b) P and r versus w with $d=30$ nm.

According to the numerically optimized results, we designed another structure of annular grooves with $d=30$ nm and $w=155$ nm, specified as *Structure 2*. The other structural parameters are the same as *Structure 1*. The field distribution measured by the probe tip with the tip-surface distance of ~ 5 nm is mapped in Fig. 6(a), and the cross-section along the dashed line in Fig. 6(a) is shown in Fig. 6(b). The measured near-field parameters are listed in Table. 1. For the convenience of comparing, the near-field parameters of *Structure 1* are also listed.

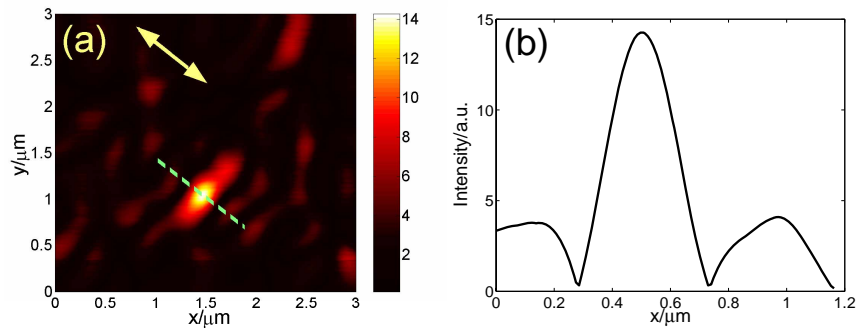


Fig. 6. Intensity distribution of the SPP field on the surface of *Structure 2* with $a=310$ nm, $L=465$ nm, $d=30$ nm and $w=155$ nm. (a) Near-field image with the tip-sample distance of ~ 5 nm. The polarization direction of the illumination is indicated by the double arrow. (b) Cross-section of (a), as indicated by the dashed line.

Table. 1 The measured near-field parameters of the two structures with the tip-sample distance of ~ 5 nm

Sample	FWHM/nm	$P/a.u.$	r
<i>Structure 1</i>	275nm (0.44λ)	11.27	45.8%
<i>Structure 2</i>	266nm (0.42λ)	14.26	40.2%

It can be seen that with d and w increasing, the maximal intensity of the central peak P is enhanced and the sidelobe suppression r is decreased. In order to observe the optimization effect more clearly, we mapped the field distributions at different tip-sample distances, and the three near-field parameters versus the distances are shown in Fig. 7. In the field distributions of the two structures, although the intensities of the central peaks attenuate and the sidelobes gain with the distance increasing, *Structure 2* weakens the tendency of deterioration. In the field distribution of *Structure 2*, the FWHM of the central peak is below 285nm (0.45λ) during 600nm distance range. At the location with tip-sample distance of 600nm, the central peak intensity P is 77% of that with tip-sample distance of ~ 5 nm (Fig. 7(b)), and the sidelobe suppression r is no more than 73% (Fig. 7(c)). All the features make the central peak still workable at 600nm away from the sample surface. Thus the distribution of the SPP field is optimized. It is worth noting that in Table. 1 and Fig. 7(a), FWHM of the central peak changes with different samples. In theory, FWHM of the interference pattern is determined by the characteristics of the gold film, such as optical constant and the thickness, and the structural parameters have little effect on it. In practice, however, the fabrication deviation of the thickness and the surface features are inevitable, consequently leading to the difference of FWHM.

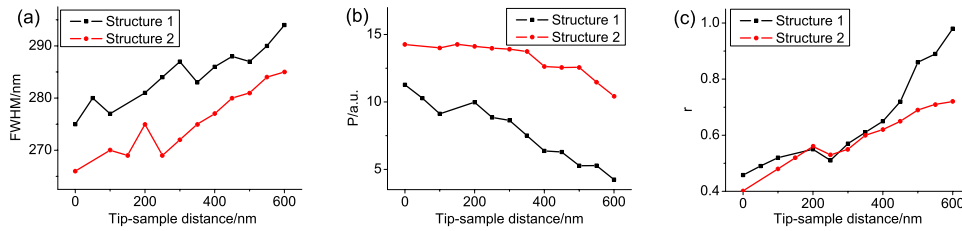


Fig. 7. Variations of the three near-field parameters versus the tip-sample distance. (a) FWHM of the central peak versus the distance. (b) The maximal intensity of the central peak P versus the distance. (c) The sidelobe suppression r versus the distance.

We have further calculated the reflectivity spectrum of the two structures to get better insight in the underlying physics of the enhancement of central peak and sidelobe suppression, which is presented in Fig. 8. It shows that a reflectivity minimum (corresponding to $\lambda=632.8$ nm) occurs in the center of the plasmonic band gap. That is the light wave of $\lambda=632.8$ nm can excite a resonant SPP defect mode in the nanocavity. Nevertheless, the dip in the reflectivity curve of *Structure 2* is deeper than that of *Structure 1*, indicating that the strongest coupling between photons and SPPs occurs at the proper values of the depth and the width of the innermost groove [34]. We believe that this strong coupling increases the performances of the SPP nanocavity, thus constitutes the main reason for the central peak enhancement and sidelobe suppression. One should therefore design carefully the SPP nanocavity structure to obtain optimized field distribution of the SPP-based near-field nano source.

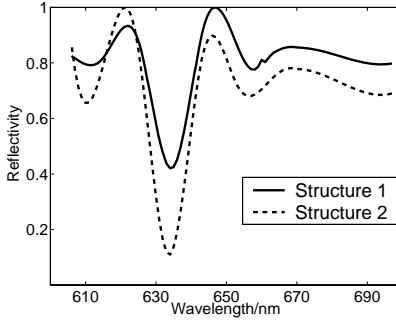


Fig. 8. The calculated reflectivity spectrum of the two structures.

4. Summary

A type of nano-confined source based on SPP Bragg reflectors and a nanocavity has been realized. The structures consisting of a nanocavity surrounded by annular grooves are used to obtain a single, localized and non-radiating central peak. The near-field characterizations show that during 600nm distance away from the sample surface, the FWHM of the central peak is below 285nm (0.45λ), and the modifications of the structural parameters of the innermost groove results in at least 1.27 times enhancement of the central peak intensity together with further sidelobe suppression (no more than 73% of the central peak intensity). All these features make the central peak workable in 600nm distance range. With the help of numerical simulations based on FDTD method, we explain the experimental findings. It is clear from this work that the structural parameters must be fully taken into account in order to optimize the SPP field distribution, and that under the proper design high quality nano source in near-field can be achieved. This type of SPP-based nano source has merits of high intensity and high sensitivity. It is promising to be applied in near-field imaging, optical manipulation, localized spectrum detection, etc, and has potential applications in nano-photonics devices based on SPP.

Acknowledgments

This research is supported by the National Natural Science Foundation of China under Grant 60678028. The authors are most grateful to Kaiwu Peng at National Nano-Center in China for FIB fabrication and fruitful technical discussions.